Heavy particles in the near field of a turbulent jet

Andrea Perrotta[a], Alessandro Capone[b,*], Giovanni Paolo Romano[a]

[a] *Dept. of Mechanical and Aerospace Engineering, Sapienza Unversity of Rome, Via Eudossiana 18, 00184, Rome, Italy*
[b] *CNR-INM, Via di Vallerano 139, Rome, Italy*

Abstract

The behaviour of aluminum spherical particles of density $\rho_p = 2700Kg/m^3$ dispersed in a turbulent round jet, at Reynolds number $Re \approx 15000$ and exit Stokes number $St_0 = 0.013$ is investigated via Particle Image Velocimetry up to $x/D = 16$ from the nozzle exit. Average and fluctuating velocity fields are analyzed and compared to the unladen jet condition. Generally, particles are reported not to behave like tracers, in particular outside the middle region of the jet potential core. Velocity fluctuations are reported to differ from the fluid fluctuations in particular at the jet centerline and shear layers suggesting a selective particle response with respect to the flow dynamics.

Keywords: Two-phase flow, Jet, Particle Image Velocimetry

2010 MSC: 76-05, 76T99, 76D25

1. Introduction

Multiphase flows, i.e. flows characterized by suspended particles transported by a fluid phase, are ubiquitous in nature and in a wide range of engineering applications. In general, multiphase flows entail several categories: solid particles dispersed in gas or liquid flows, droplets in gaseous streams and liquid flows with bubbles. The high level of complexity of the interactions occurring between the turbulent flow and the dispersed phase is usually tackled by focusing separately on the two-fold relationship between the two phases. On one

*Corresponding author
Email address: alessandro.capone@inm.cnr.it (Alessandro Capone)

side, the effect of turbulent flow on the dispersion and concentration of the dispersed phase, summed up by the term "preferential concentration" ([1]); on the other, the turbulence modulation effects brought about by the suspended phase on the carrier flow (see [2] for a comprehensive review of both aspects). Based on the type and extent of such interactions, the dynamic coupling between dispersed and carrier phase is defined as one-way, two-way coupling and four-way coupling. The former, which according to [3] is limited to particle suspensions featuring a volume fraction $\phi_p = V_p/V < 10^{-6}$, where V_p and V are the volume of the dispersed phase and the total volume respectively, describes a system where only the fluid exerts an action on the dispersed phase, whereas turbulence modulation effects are negligible. Two-way coupling regime occurs for $10^{-6} < \phi_p < 10^{-3}$ and characterizes suspensions where the dispersed phase concentration is high enough to generate an exchange of momentum between phases thus activating extra mechanisms of turbulence production and dissipation. For higher ϕ_p four-way coupling regime is considered, where in addition to the above phenomena, inter-particle interaction are not negligible. This regime is not discussed hereafter in this work, whereas we will focus on the two-way coupling regime.

A particular class of multiphase flow which is of interest to fundamental research and is encountered in a wide range of industrial processes is that of particle-laden turbulent round jets. Occurrences are found in spray, combustion applications as well as for cooling purposes. Despite the apparent straightforward features, the behaviour of particle-laden jets is dominated by several parameters whose interleaved effect on the resulting flow and particle dynamics is yet to be fully understood. In their review work, [2] identify at least four parameters which govern the extent of mutual interactions between phases in a two-way coupled suspension: the Stokes number St defined as the ratio of a particle relaxation time τ_p to a flow time scale τ_f; the ratio of the particle to fluid density ρ_p/ρ_f; the particle Reynolds number $Re_p = (u_f - u_p)\rho_f d_p/\mu$ based on the particle-to-fluid slip velocity $u_p - u_f$ and the ratio of the particle length

scale (the particle diameter d_p for spherical particles) to the Kolmogorov turbulent length scale. As a matter of fact, a comprehensive study which entails all of the mentioned parameters is extremely difficult and all of the existing literature on the subject is focused on a limited aspect and set of variables. Based on the following definitions

$$\tau_p = \frac{(2\rho_p + \rho_f)d_p^2}{36\mu} \tag{1}$$

$$\tau_f = \frac{D}{U_b} \tag{2}$$

where D and U_b are respectively the jet exit diameter and the jet exit bulk velocity, the corresponding range of jet exit Stokes number St_0 reported in literature is, to the Authors' knowledge, approximately $10 < St_0 < 70$, whereas for the density ratio $\rho_p/\rho_f >> 1$ holds true.

Many efforts have been put forward in the past years to investigate on particle-laden jets in a range of configurations both by simulations ([4], [5], [6] [7] among others) and by experiments. From the point of view of the latter, the analysis of turbulent particle-laden flows poses difficult challenges to the researcher; if measurements are to be collected on both the carrier and dispersed phase, advanced methodologies should be employed. The most widespread and successful techniques adopted to deal with these flows are Laser Doppler Anemometry, herafter LDA ([8],[9] among others) and Particle Image Velocimetry, hereafter PIV ([10]). The latter has currently superseded other techniques due to the potential to carry out simultaneous velocity measurement of both phases over a non-pointwise acquisition area.

Early works by [11],[12] and [13] analyze air jets laden with glass or polystyrene beads by means of LDA reporting marked differences between the mean axial velocity profiles and fluctuations of particles and fluid. In [14], the Authors considered the same configurations while testing a wider range of particle diameters. By acoustically forcing an air jet [15] thoroughly investigated the preferential concentration of dispersed glass beads in a turbulent air jet by

proposing a model for coherent structures/particle interactions. More recently, Phase Doppler Anemometry (PDA) was employed in [9] and [16] to attain simultaneous flow/particle velocity measurement. This optical method detects the light scattered by an individual particle and determines its velocity from the signal frequency shift as in conventional LDA. By using multiple detectors it is also possible to determine the particle diameter.

In a recent comprehensive work [17] focus onto the lower St_0 number range, with the aim to better understand the dependence of particle dispersion and velocity on this parameter. In this paper, by using PIV combined with Particle Nepherometry (PN), an air jet laden with glass beads in the range $0.4 < St_0 < 11$ is investigated, as attained by adjusting the jet exit velocity U_b. According to [1], within this St_0 range, preferential concentration effects are enhanced. A non-exhaustive summary of numerical and experimental studies on turbulent jets laden with heavier-than-fluid particles is provided in Table 1.

Study	Re	St_0	ρ_p/ρ_f
Eaton and Longmire (1994) [1]	19000-23000	NA	2000
Fan et al. (1997) [18]	>44300	8.3,12.4	NA
Fleckhouse et al. (1987) [11]	20000	62.5,265.9	2158
Frishman et al. (1999) [19]	>30000	24.4,70.2	3292
Gillandt et al. (2001) [16]	4750	39	2000
Prevost et al. (1996) [9]	13100	19.8	2158
Zhou et al. (2016) [6]	4500	0.01-50	2000
Casciola et al. (2010) [7]	2000	2-128	1000
Luo et al. (2013) [5]	3000	0.5-67.75	2000
Lau and Nathan (2014) [17]	10000-40000	0.3-22.4	1000

Table 1: Summary of numerical and experimental studies on turbulent jets laden with heavier-than-fluid particles. Some data are inferred indirectly and obtained from [17].

To the present Authors' knowledge, there is a lack of experimental work on the behaviour of dispersed particles in a turbulent jet with moderate density

ratios ($1 < \rho_p/\rho_f < 10$). Nonetheless, the effects of such ratios, and in turn of the ratio of particles mass to the overall mass $\phi = M_p/M_t$, is known to be relevant to determine the extent of the particle/fluid dynamic interactions ([2]). In this work, we aim at partially covering this gap, by investigating a turbulent round water jet laden with aluminum spherical particles ($\rho_p = 2700Kg/m^3$) at jet exit Stokes number $St_0 = 0.013$. While this latter value is usually considered representative of dispersed particles following faithfully the flow dynamics, its intertwined role in combination with conditions characterized by moderate ρ_p/ρ_f has not been addressed yet. Furthermore, we point out that the choice of a unique flow time scale τ_f when dealing with a turbulent flow is necessarily limited ([9]), as it does not take into account the wide range of scale down to the Kolmogorov scale.

In order to obtain whole-field, high spatially resolved data, we employ PIV as measurement method. Particle velocity statistics are obtained and compared to the unladen case. Use of PIV for investigation of multiphase flows is quite recent and is steadily spreading due to its intrinsic capability to obtain high spatially resolved measurement data in a relatively short time compared to single-point measurement provided by LDA and PDA ([20], [21]). Nonetheless, just a handful of works have tackled turbulent particle-laden jet flows with this technique and the results presented serve as further evidence of the effectiveness of its effectiveness in the investigation of turbulent multiphase flows.

2. Experimental setup

2.1. Experimental facility

The experimental apparatus is schematically described in Figure 1. A pipe with a diameter $D = 2\,\text{cm}$ is placed vertically, to avoid gravity bias, and discharges into a $66D \times 45D \times 50D$ water tank so that flow is in the direction of gravity. An additional suspended tank is used to feed the pipe with solid particles. By regulating the water level a constant flow rate is attained, such

that the exit bulk velocity, U_b, is equal to $1\,\mathrm{m\,s^{-1}}$, yielding a Reynolds number

$$\mathrm{Re} = \frac{U_b D}{\nu} \approx 15000. \tag{3}$$

The tank dimensions are large enough for the jet to be deemed unconfined, in fact following the equation for the momentum decay provided by Hussein et al. [22]

$$\frac{M}{M_0} = \left[1 + \frac{16}{\pi B^2}\left(\frac{x}{D}\right)^2 \frac{A_0}{A_t}\right]^{-1}, \tag{4}$$

where $M = \int u\,dA$ is the momentum, A_0 and A_t respectively the cross-sectional area of the pipe and of the tank, $B = 6.5$ the decay coefficient of the axial velocity, we obtain at $x/D = 20$ a momentum ratio $M/M_0 \approx 0.98$.

Aluminum spherical particles with diameters between 30 and 40 µm are mixed in water within a pressurized bin and injected with a flow rate of around $20\,\mathrm{mL\,min^{-1}}$, which is negligible with respect to the flow rate of the main pipe, by means of a t-junction to the main pipe. The aluminum particles concentration within the feeding bin was calibrated in order to obtain the desired volume fraction $V_p/V = \Phi_p \approx 10^{-5}$. The particle volume $V_p = M_p/\rho_p$ is determined by mixing a known particle mass M_p inside the pressurized bin. The total volume is obtained by the expression $V = V_p + V_fp + V_{fb}$, where the latter two terms represent the volume of fluid which flows through the pipe during the acquisition time window and the volume of fluid inside the pressurized bin, respectively. Since V_fp depends directly on the constant flow rate and the acquisition time of each run, the corresponding particle mass M_p to be inserted into the bin is determined in order to obtain the desired $\phi_p \approx 10^{-5}$. We point out that the acquisition time is set according to the number of image pairs necessary to attain statistical convergence of the results, as set out in more detail in the next section. Based on the previous discussion, we can expect a two-way coupling regime between dispersed and carrier phases to take place under these conditions. With regards to the St_0 calculation, as described in the previous section, based on equation (1) it is obtained $St_0 = 0.013$. We point out that this formulation is valid for low particle Reynolds numbers Re_p. A preliminary and

rough estimate of the slip velocity $U_s = U_f - U_p$ is obtained via the terminal velocity equation

$$U_s = \frac{2g(\rho_p - \rho_f)d_p^2}{36\mu}, \tag{5}$$

valid in the creeping-flow approximation, where μ is the dynamic viscosity of the fluid and g the gravitational acceleration. It descends that $Re_p << 1$ and thus the creeping flow approximation is acceptable ([23], [24]).

The pipe total length is $L_p = 2.5m$, leading to a length-to-diameter ratio of $L_p/D \geq 125$. As regards single-phase, i.e. unladen flow, the mentioned ratio is large enough for a fully developed jet exit profile to develop ([25, 26, 27]). For particle-laden acquisition, a t-junction is adopted to inject the dispersed phase, as shown in Figure 1, located approximately $50D$ from the pipe exit. This considered, as regards the necessary pipe length to establish a fully developed suspension, no systematic study has been performed, as also reported by [17]. Similar works ([20]) with non-homogeneous dispersed particles have shown that the current configuration can ensure that fully developed conditions are reached. Separate acquisition are carried out: single-phase flow which serves as a benchmark and setup validation and particle-laden flow where particles are injected without the presence of tracers.

2.2. PIV system

A Nd:YAG laser source, (532 nm) with a repetition frequency of 5 Hz was employed. For single-phase measurements, water was seeded with neutrally buoyant hollow glass spherical tracers with a mean diameter equal to 10 µm. Images were acquired by means of a PCO 4000 cross-correlation camera with a resolution of 4072×2720 pixels placed orthogonally to the plane of light. The camera mounted a Nikon f=50 mm objective and a 48 mm extension tube in order to zoom-in the field of view. The laser sheet thickness was approximately 1 mm. The imaged area was 70 mm × 105 mm that corresponds to $3.5D \times 5.25D$. Six partially overlapped regions were acquired in order to investigate the near-field region, thus an overall distance from the pipe exit of around $16D$ was investigated. For each single region acquisition 1000 image pairs were collected

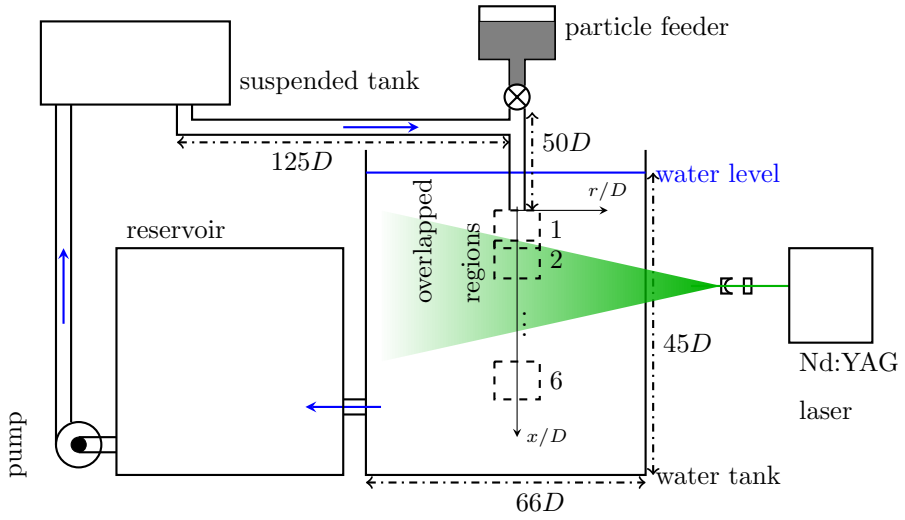

(a) side view xr-plane

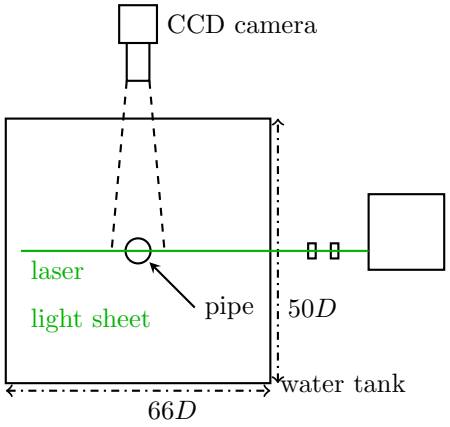

(b) top view $r\theta$-plane

Figure 1: Schematics of the experimental setup.

in order to attain statistical convergence. The flow and particle velocity fields are obtained following a series of steps: image pre-processing, processing (cross-correlation) and vector validation. Image pre-processing is carried out in order to improve the effectiveness of the next cross-correlation step and consists of two stages. Firstly, images are background-subtracted by calculating a minimum intensity image, over the acquired images set, at single-pixel level. Secondly, such images are processed with a spatial high-pass filter with a threshold of 16 pixels in order to sharpen the image.

The cross-correlation step is performed via the PivLab package, which implements a multi-pass, FFT windows deformation, cross-correlation algorithm (William Thielicke [28]). Optimal sub-windows grid resolution is set to 64 x 64 pixels for the first pass and second pass and 32 x 32 pixels and 16 x 16 pixels for the third and final pass. The resulting vector grid spacing is 8 pixels (a sub-window overlap of 50% was set), which corresponds to approximately $0.003D$. As mentioned before, the presented setup made it possible to achieve high spatial resolution with a marked improvement compared to existing literature.

Data were validated applying both a global standard deviation filter with threshold of 3 standard deviations and a local median filter (3x3 points kernel) with threshold 3 standard deviations. With 1000 image pairs for each acquisition region, the uncertainty affecting the average fields is estimated, based on the Student t-distribution, to be within $\pm$ 1.2% of the measured data with a confidence interval of 95%. Following [29], the uncertainty of RMS measurements is estimated to be within the interval $\pm$ 4.6%. Error bars reported in plots are displayed accordingly. It is worthwhile pointing out that the subject of the non-homogeneous velocity of inertial particles within PIV interrogation window has been tackled by [30] who compared the velocity of inertial particles obtained from PIV to those by particle tracking in an impinging jet configuration. They showed that the only flow regions where a mismatch in the two measurements were detectable and PIV results were not faithful to the actual particles velocity were those characterized by a dominant, but not exclusive, particle trajectory. Based on this evidence and since the experimental set-up presented

in this work does not feature such critical regions, we can safely consider the velocity statistics obtained from PIV a reliable estimate of the actual particles velocity. Sensitivity analysis of the velocity measurements to the correlation window size confirms that convergence is attained with the chosen size, namely 16-pixel windows.

3. Results and discussion

In this section the features of the velocity field of the unladen, single phase jet are analyzed and compared to the results of the laden case. As mentioned before, only the dispersed particles velocity field is measured in this case, although hereafter we will refer to it as two-phase case. Therefore, it is not possible to obtain information about the possible turbulence modulation effects which could take place. Nonetheless, this approach has been proven to provide valuable information about the interactions among the turbulent flow and the dispersed particles, as reported in [31]. It is interesting to point out that the latter also discuss the significance of the pseudo slip velocity, obtained by comparing the flow single-phase velocity to the particle velocity.

3.1. Average velocity fields and particle concentration

In Fig. 2, the outlet average velocity profiles of the single phase and two phase jets are reported with reference to PIV data obtained by Capone et al. [32] and cold-wire data from Mi et al. [33]. We point out that results from Capone et al. [32] are at a different Reynolds number and pipe geometry from the current experiment. At the pipe exit the velocity profile should be comparable with the one inside the pipe, therefore a typical reference solution is the empirical $1/n$ power law, with $n = 6.5$

$$\frac{U}{U_e} = \left(1 - 2\frac{r}{D}\right)^{1/n} \tag{6}$$

where $U =< u >$ is the mean axial velocity, U_e is the maximum exit velocity and r/D the dimensionless radial direction. These reference values as well as the present ones are actually extracted at $x/D = 0.01$. It can be noticed that

the peak exit velocity is on average the same for the unladen jet and dispersed particles. This is in contrast with the results reported by [21] ($St_0 \approx 1$, $\rho_p/\rho_f \approx 1$) and [17] ($St_0 = 0.3$, $\rho_p/\rho_f \gg 1$) where dispersed particles were reported to lag the fluid at jet exit. This confirms that particles motion at the jet centerline is slightly affect by their inertia but rather is dominated by the surrounding flow, as it is suggested by the current St_0. On the other hand, along the radial direction, from $r/D \approx 0.6$, particles velocity profile departs from single phase conditions, featuring higher values. This behaviour resembles that reported in [13], though at a lower extent, and in [21] where non-spherical particles are dispersed. Therefore it is found that in conditions characterized by ρ_p/ρ_f higher than unity, particles depart locally from the carrier fluid velocity profile, even at low St_0. It is worth pointing out that this occurs just outside the middle region of the jet potential core.

As a confirmation of the creeping-flow approximation, a pseudo slip velocity is obtained by considering the difference between the two-phase and single-phase velocities, in a similar fashion as [17]. It is obtained that the particle Reynolds number does not exceed that value $Re_p = 3 * 10^{-4}$ thus the creeping-flow approximation may be deemed valid. It is shown in Fig. 3 that as the jet develops to the self-similarity region, [34]) the scaled radial profiles of the single phase and laden cases well fit the gaussian profile [22]

$$\frac{U}{U_c} = e^{-\log(2)\left(\frac{r}{r_{1/2}}\right)^2} \tag{7}$$

where U_c is the centreline velocity as a function of the axial position and $r_{1/2}$ is the local jet half-radius, which is determined by the equation $U_{r_{1/2}} = U_c/2$. The observation of a substantial equivalence among results of single and two-phase flow points out that as the jet develops, the average motion of the dispersed particles is dominated by the surrounding fluid as for the single-phase je

The evolution of the jet axial velocity U_e is investigated in Fig. 4 where the trend of its inverse normalized by U_c is shown for single-phase and particle laden cases. It is known that the centreline axial velocity remains constant up to an axial distance of approximately $5D$ from the jet exit whereas further

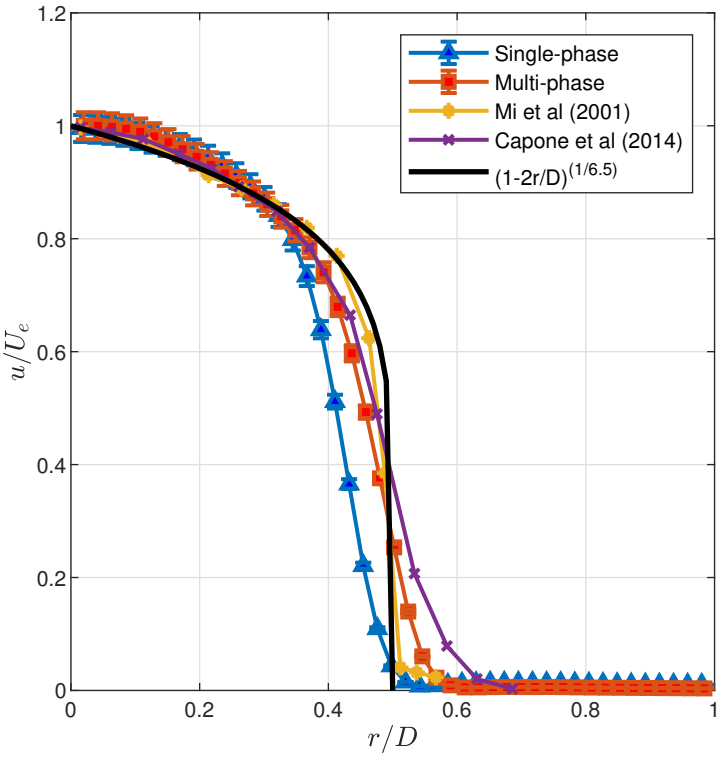

Figure 2: Radial profile of the mean, axial velocity at the pipe exit ($x/D = 0.01$ for experimental data) normalized with respect to the exit velocity U_e, for the single-phase and laden cases and comparison to literature data and power law (Eq. (6)) with $n = 6.5$. Error bars, partially covered by symbols, specify a 95% confidence interval.

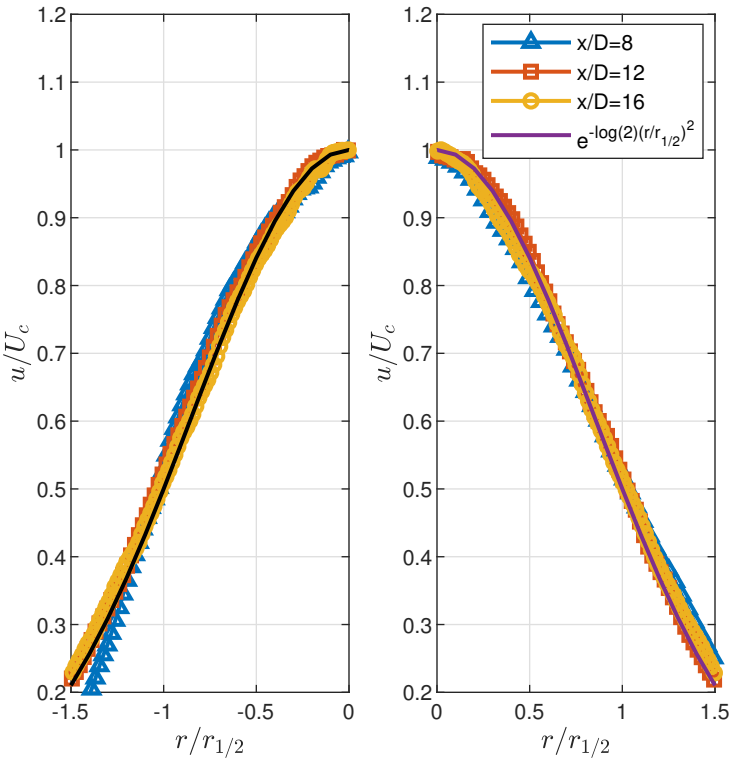

Figure 3: Radial profile of the mean, axial velocity normalized with respect to the centreline velocity and scaled with respect to the jet half-radius, for three axial distance and compared with the gaussian solution. Two-phase (left) and single-phase (right).

downstream it follows the law ([34])

$$\frac{U_e}{U_c} = \frac{1}{B}\frac{x - x_0}{D} \tag{8}$$

where B is the decay coefficient, already introduced in Sec. 2.1, and x_0 is the virtual origin. While there is a good agreement for the possible values of the decay coefficient, from 4.48 to 6.7 [35], values for the virtual origin reported in literature can instead vary from -2 to 7 [36] as dependent on initial and boundary conditions. From Fig. 4 it is obtained that $x_0 = -0.23 \pm 0.03$ for the single phase case and $x_0 = -0.8 \pm 0.01$ for the two phase case, whereas B coefficient is almost the same for both conditions: $B = 5.08 \pm 0.06$ for the single phase and $B = 4.97 \pm 0.06$ for the two phase. It descends that dispersed particles spread very similarly to the single-phase flow whereas within the transition zone (approximately between $4D$ and $7D$) their inertia still affects their distribution. These findings are in apparent contrast to those by [17], where particles with exit Stokes number of an order of magnitude higher than the current ones were reported to follow the linear trend for approximately $x/D > 5$. The delay in the linear trend onset may be attributed to the effect of the lower particle-to-fluid density ratio.

Further insight into the evolution of the axial decay may be provided by the inspection of the local Stokes number, calculated with the following approximated formula by [17]

$$St_U \approx St_0 \left(\frac{D/2}{r_{1/2}}\right)\left(\frac{U_c}{U_e}\right) \tag{9}$$

and plotted in Fig. 4. Similar to the findings by [17], it is reported that the fastest decay rate of St_U occurs within the transition range of the jet, after which the decrease rate is markedly reduced.

Particle concentration profile is estimated by following a similar approach to [17], where the same images employed for PIV measurements are used. Relative concentration is then estimated based on the intensity of the measured Mie scattering signal. In Fig. 5 the concentration thus obtained C is plotted at the jet exit, normalized to the bulk value C_b. It appears that particles feature a

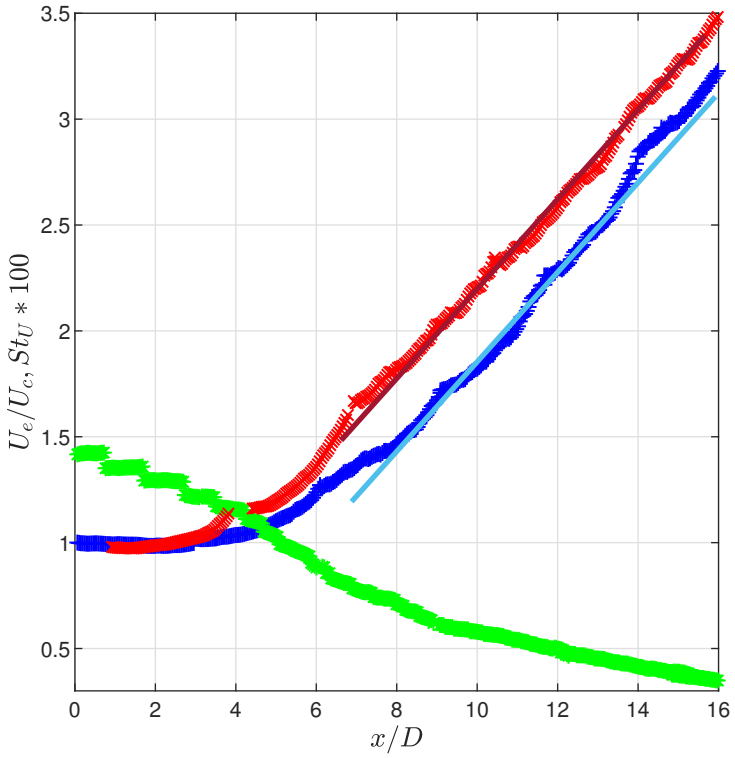

Figure 4: Axial evolution of the inverse centreline axial velocity normalized with respect to the exit axial velocity for two-phase (red) and single-phase (blue) and local Stokes number Sk_U (green).

tendency to concentrate around the axial region of the jet, with particles exceeding the bulk concentration within the approximate range $-0.35 < x/D < 0.35$. Comparison to literature data from [17] and [12] reveals that the investigated particles behave similarly to higher Stokes number particles.

3.2. Fluctuating fields

In this section, the normal and mixed Reynolds stresses are discussed for the single and two-phase case. In Fig. 6, the root mean square (RMS) of the axial and vertical component of velocity u' and v' along with the mixed Reynolds stress $< uv >$ are plotted normalized respectively to exit velocity U_e

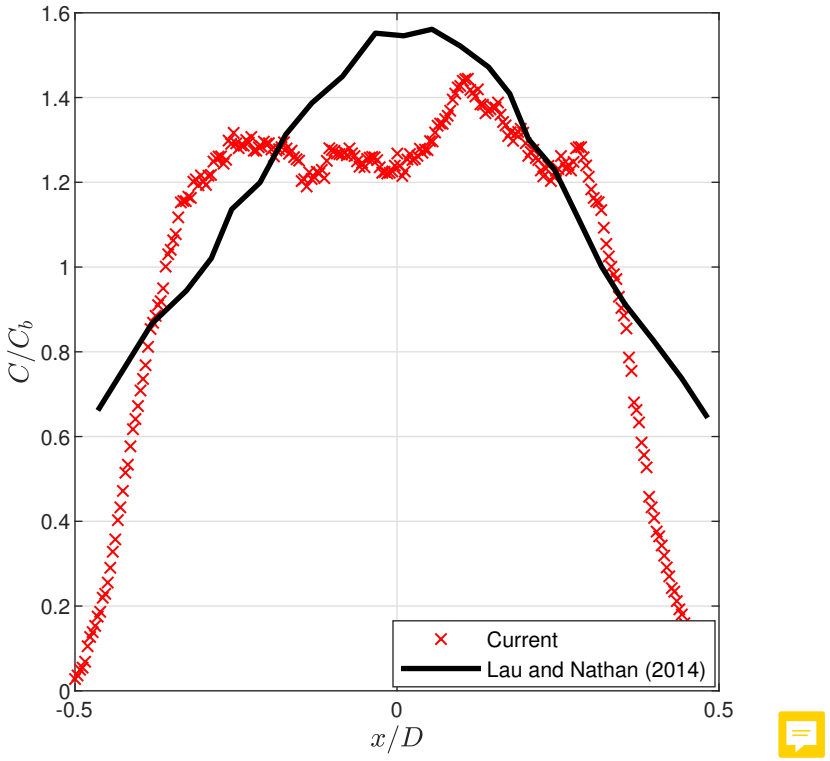

Figure 5: Normalized particle concentration C/C_b at jet exit compared to reference data from [17].

and ${U_e}^2$. The fluctuations of the laden case, normal and mixed, are lower than the single-phase starting from $x/D \approx 8$. In addition, the loci of maxima have been extracted by interpolating the data in order to analyze the evolution of the shear layer along the axial direction, reported in Fig. 7. Peak axial velocity fluctuations decreases almost monotonically after the potential core region, with closely similar behaviour of the unladen case and dispersed particles, with an overall downstream displacement for the single phase data (Fig. 7, middle). This is confirmed by the peak radial velocity fluctuations which show a maximum of the same magnitude for the single phase case at $x/D \approx 10$ and for dispersed phase case at $x/D \approx 7.5$ (Fig. 7, top). The mixed Reynolds stress

trend features a similar behavior.

Results in Fig. 8-9, where the radial profiles of u' and v' within the potential core have been reported, show that the dispersed phase is characterized by reduced velocity fluctuations at the centreline but enhanced fluctuations within the shear layer region. This is partly in agreement with findings from [17] where, at the lowest St_0 tested, particles were reported to have comparable level of fluctuations at the centerline as opposed to the shear layer region. It can be inferred that for increasing density ratio this behaviour would be enhanced. Additionally, we point out that the ratio ρ_p/ρ_f is reported by [37] to have a marked impact on the frequency response of the particles and consequently could act selectively to the different temporal scales featured by the flow.
Turbulent kinetic energy $k = 1/2(u'^2 + v'^2 + w'^2)$ can be computed by assuming for symmetry reasons $k = 1/2u'^2 + v'^2$ and presented as $(2k/3)^{1/2}$ in Fig. 10 in order to be comparable with u', as suggested by Amielh et al. [38]. It is noteworthy that the kinetic turbulent energy of the dispersed particles is lower than the single-phase case for $x/D < 2.5$, then it becomes higher for $4 < x/D <$ 10.

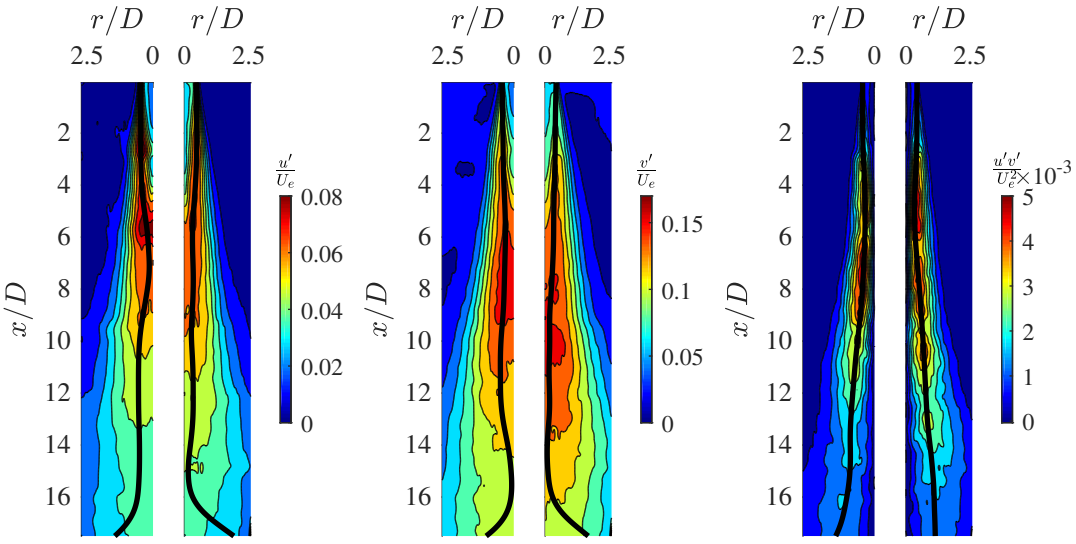

(a) two phase (b) single phase (c) two phase (d) single phase (e) two phase (f) single phase

Figure 6: Contours of the RMS u', v' and the mixed Reynolds stress $< uv >$. The black lines indicate the loci of maxima

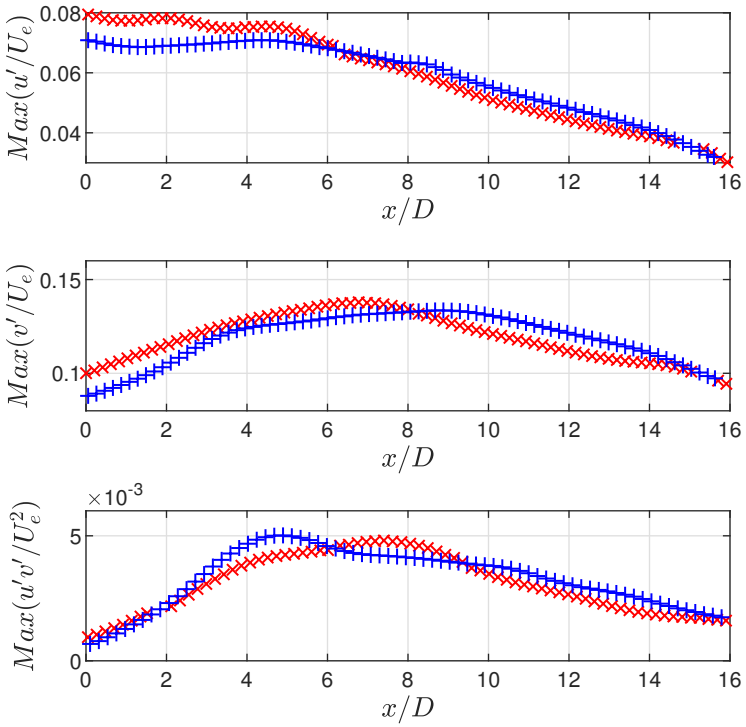

Figure 7: Axial evolution of u', v' and $u'v'$ along the black lines indicated in Fig. 6. Single-phase (blue +) and two-phase (red X).

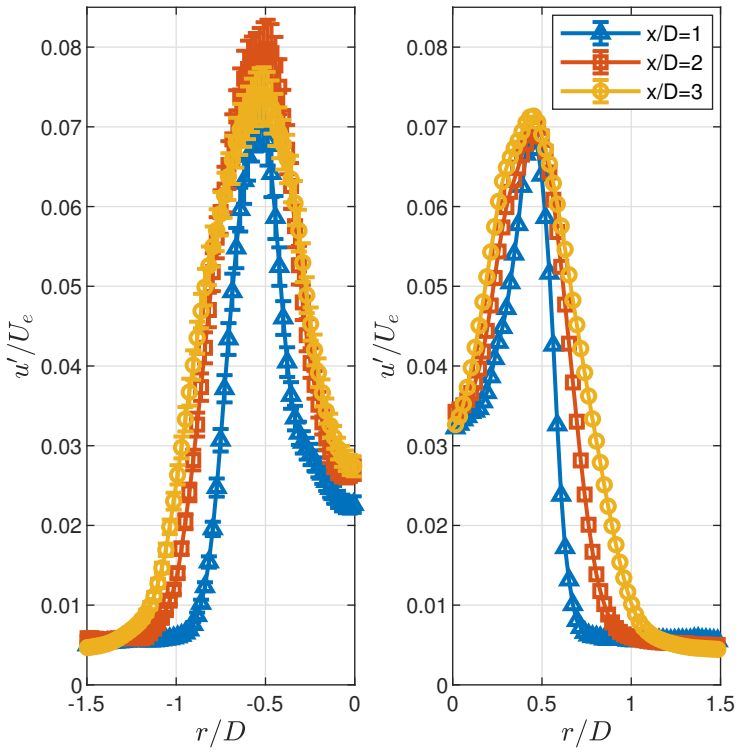

Figure 8: Radial profiles of u'. Two-phase (left) and single-phase (right). Error bars specify a 95% confidence interval.

4. Summary and conclusions

The features of the velocity field related to solid particles, i.e. ~~of~~ aluminum spherical particles (particle to fluid density ratio $\rho_p/\rho_f = 2.7$), dispersed in a turbulent water jet were investigated via Particle Image Velocimetry at a Reynolds number $Re \approx 15000$. Average and fluctuating quantities were analysed in the single phase, unladen case and compared to the dispersed particles characteristics. Mean trends show that particles velocity departs from the single-phase case outside the potential core and within the transition region of the jet. As the fully-developed region is approached, particles exhibit a self-similar velocity profile. In contrast to some literature results for very high ρ_p/ρ_f particles,

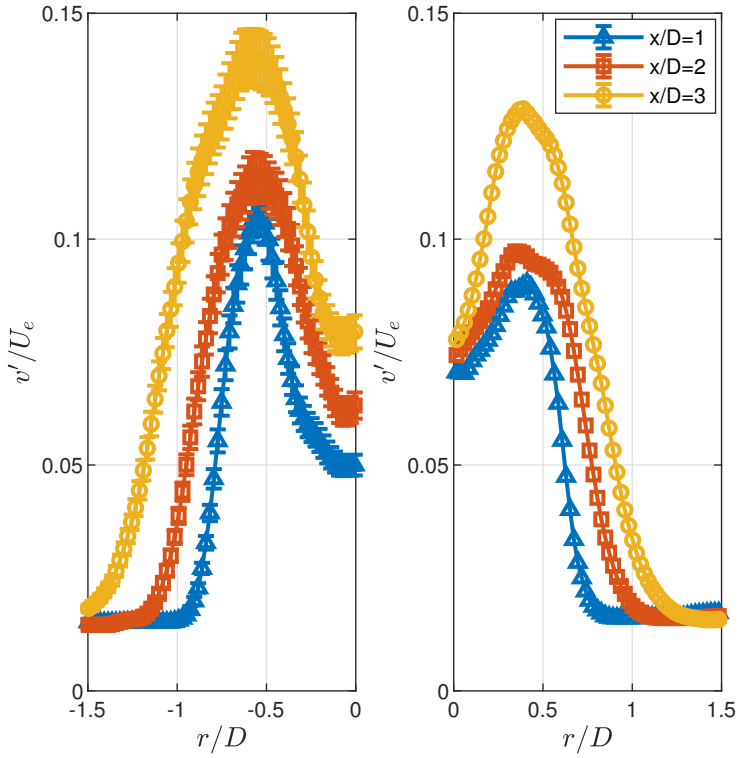

Figure 9: Radial profiles of v'. Two-phase (left) and single-phase (right). Error bars specify a 95% confidence interval.

the current particles are characterized by an extended transition region. Analysis of velocity component RMS and mixed Reynolds stress reveals that along the axial direction particles tend to have a different behaviour in the jet region before $x/D = 5$, whereas their trend resembles the single phase farther downstream, with the exception of the radial fluctuations. Along the radial direction, particles exhibit lower and higher turbulence levels respectively close to the centerline and in the shear layers compared to the unladen case. These results should be interpreted in the light of the frequency response of the particles, which in turn is strongly dependent on the particle-to-fluid density ratio. With this respect, very high ρ_p/ρ_f particles are expected to exhibit a low-pass

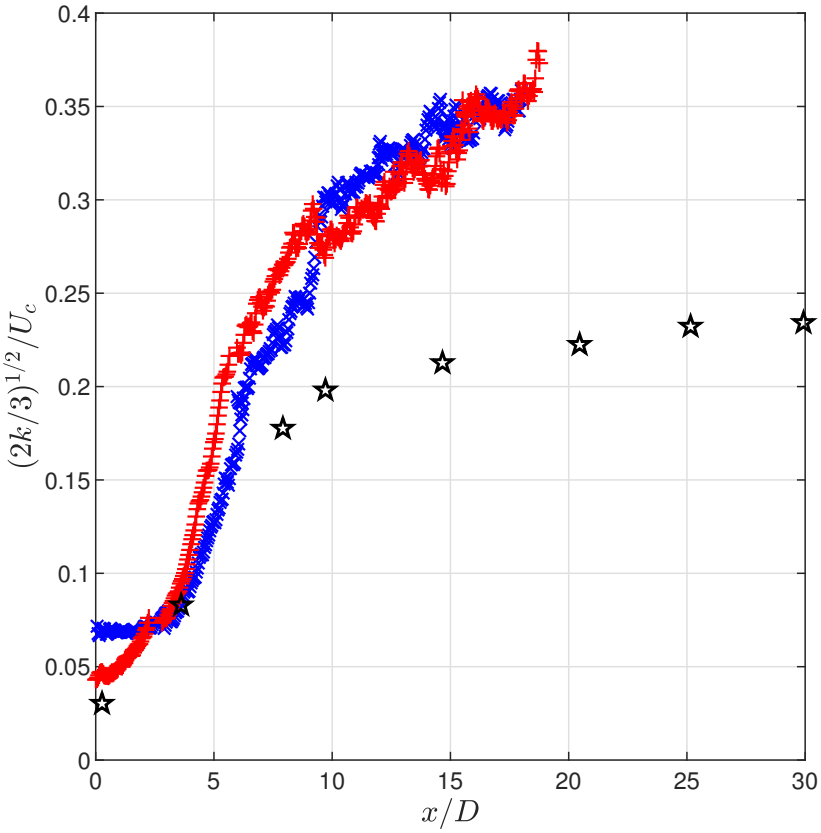

Figure 10: Axial evolution of the centreline kinetic turbulent energy. Single-phase (blue X), two-phase (red +) and reference data from Xu and Antonia [39] (black stars). Reference values by Xu and Antonia [39] refer to u'/U_c

character more marked than the investigated particles, although they cannot be deemed faithful tracers. These results show that moderately heavy particles with low exit Stokes number display a non-trivial behaviour in turbulent multi-phase flows. It appears that in these conditions the sole Stokes number cannot be representative of the reported dynamic behaviour. With this respect, additional work will be necessary to investigate the role played by the density ratio in such conditions.

References

[1] J. K. Eaton, J. Fessler, Preferential concentration of particles by turbulence, International Journal of Multiphase Flow 20 (1994) 169–209.

[2] S. Balachandar, J. K. Eaton, Turbulent dispersed multiphase flow, Annual review of fluid mechanics 42 (2010) 111–133.

[3] S. Elghobashi, On predicting particle-laden turbulent flows, Applied Scientific Research 52 (4) (1994) 309–329, ISSN 1573-1987, doi:10.1007/BF00936835.

[4] J. Chung, T. Troutt, Simulation of particle dispersion in an axisymmetric jet, Journal of Fluid Mechanics 186 (1988) 199–222.

[5] K. Luo, N. Gui, J. Fan, K. Cen, Direct numerical simulation of a two-phase three-dimensional planar jet, International Journal of Heat and Mass Transfer 64 (2013) 155–161.

[6] H. Zhou, G. Mo, K. Cen, Numerical investigation of a gas–solid turbulent jet flow with Reynolds number of 4500 using lattice Boltzmann method, Applied Mathematical Modelling 40 (1) (2016) 565–577.

[7] C. Casciola, P. Gualtieri, F. Picano, G. Sardina, G. Troiani, Dynamics of inertial particles in free jets, Physica Scripta 2010 (T142) (2010) 014001.

[8] C. Rogers, J. Eaton, The effect of small particles on fluid turbulence in a flat-plate, turbulent boundary layer in air, Physics of Fluids A: Fluid Dynamics 3 (5) (1991) 928–937.

[9] F. Prevost, J. Boree, H. Nuglisch, G. Charnay, Measurements of fluid/particle correlated motion in the far field of an axisymmetric jet, International Journal of Multiphase Flow 22 (4) (1996) 685–701.

[10] T. Oakley, E. Loth, R. Adrian, A two-phase cinematic PIV method for bubbly flows, Journal of Fluids Engineering 119 (3) (1997) 707–712.

[11] D. Fleckhaus, K. Hishida, M. Maeda, Effect of laden solid particles on the turbulent flow structure of a round free jet, Experiments in Fluids 5 (5) (1987) 323–333.

[12] Y. Tsuji, Y. Morikawa, T. Tanaka, K. Karimine, S. Nishida, Measurement of an axisymmetric jet laden with coarse particles, International Journal of Multiphase Flow 14 (5) (1988) 565–574.

[13] C. Zoltani, A. Bicen, Velocity measurements in a turbulent, dilute, two-phase jet, Experiments in fluids 9 (5) (1990) 295–298.

[14] Y. Hardalupas, A. Taylor, J. H. Whitelaw, Velocity and particle-flux characteristics of turbulent particle-laden jets, Proceedings of the Royal Society of London. A. Mathematical and Physical Sciences 426 (1870) (1989) 31–78.

[15] E. K. Longmire, J. K. Eaton, Structure of a particle-laden round jet, Journal of Fluid Mechanics 236 (1992) 217–257.

[16] I. Gillandt, U. Fritsching, K. Bauckhage, Measurement of phase interaction in dispersed gas/particle two-phase flow, International Journal of Multiphase Flow 27 (8) (2001) 1313–1332.

[17] T. C. Lau, G. J. Nathan, Influence of Stokes number on the velocity and concentration distributions in particle-laden jets, Journal of Fluid Mechanics 757 (2014) 432–457.

[18] J. Fan, K. Luo, M. Y. Ha, K. Cen, Direct numerical simulation of a near-field particle-laden plane turbulent jet, Physical Review E 70 (2) (2004) 026303.

[19] F. Frishman, M. Hussainov, A. Kartushinsky, Ü. Rudi, Distribution characteristics of the mass concentration of coarse solid particles in a two-phase turbulent jet, Journal of aerosol science 30 (1) (1999) 51–69.

[20] A. Capone, G. P. Romano, Interactions between fluid and fibers in a turbulent backward-facing step flow, Physics of Fluids 27 (5) (2015) 053303.

[21] A. Capone, G. P. Romano, A. Soldati, Experimental investigation on interactions among fluid and rod-like particles in a turbulent pipe jet by means of particle image velocimetry, Experiments in Fluids 56 (1) (2015) 1.

[22] H. J. Hussein, S. P. Capp, W. K. George, Velocity measurements in a high-Reynolds-number, momentum-conserving, axisymmetric, turbulent jet, Journal of Fluid Mechanics 258 (1994) 31–75, doi:10.1017/S002211209400323X.

[23] G. Hetsroni, Particles-turbulence interaction, International Journal of Multiphase Flow 15 (5) (1989) 735 – 746, ISSN 0301-9322, doi:10.1016/0301-9322(89)90037-2.

[24] C. Crowe, J. Chung, T. Troutt, Particle mixing in free shear flows, Progress in energy and combustion science 14 (3) (1988) 171–194.

[25] M. M. Enayet, M. M. Gibson, A. M. K. P. Taylor, M. Yianneskis, Laser-Doppler measurements of laminar and turbulent flow in a pipe bend, International Journal of Heat and Fluid Flow 3 (4) (1982) 213–219, doi:10.1016/0142-727X(82)90024-8.

[26] J. Azzola, J. A. C. Humphrey, H. Iacovides, B. E. Launder, Developing Turbulent Flow in a U-Bend of Circular Cross-Section: Measurement and Computation, Journal of Fluids Engineering 108 (2) (1986) 214–221.

[27] E. Ferdman, M. V. Oslash, t uacute, gen, S. Kim, Effect of Initial Velocity Profile on the Development of Round Jets, Journal of Propulsion and Power 16 (4) (2000) 676–686, doi:10.2514/2.5627.

[28] E. J. S. William Thielicke, PIVlab - Towards User-friendly, Affordable and Accurate Digital Particle Image Velocimetry in MATLAB, Journal of open research software .

[29] J. S. Bendat, A. G. Piersol, Random data: analysis and measurement procedures, vol. 729, John Wiley & Sons, 2011.

[30] S. Anderson, E. K. Longmire, Interpretation of PIV autocorrelation mesurements in complex particle-laden flows, Experiments in fluids 20 (4) (1996) 314–317.

[31] T. C. Lau, G. J. Nathan, A method for identifying and characterising particle clusters in a two-phase turbulent jet, International Journal of Multiphase Flow 88 (2017) 191 – 204, ISSN 0301-9322, doi:10.1016/j.ijmultiphaseflow.2016.10.002.

[32] A. Capone, G. P. Romano, A. Soldati, Experimental investigation on interactions among fluid and rod-like particles in a turbulent pipe jet by means of particle image velocimetry, Experiments in Fluids 56 (1) (2014) 1, ISSN 1432-1114, doi:10.1007/s00348-014-1876-4.

[33] J. Mi, D. S. Nobes, G. J. Nathan, Influence of jet exit conditions on the passive scalar field of an axisymmetric free jet, Journal of Fluid Mechanics 432 (2001) 91–125, doi:DOI:undefined.

[34] S. B. Pope, Turbulent flows, 2001.

[35] C. Ball, H. Fellouah, A. Pollard, The flow field in turbulent round free jets, Progress in Aerospace Sciences 50 (2012) 1 – 26, ISSN 0376-0421, doi:10.1016/j.paerosci.2011.10.002.

[36] A. Vouros, T. Panidis, Turbulent properties of a low Reynolds number, axisymmetric, pipe jet, Experimental Thermal and Fluid Science 44 (2013) 42 – 50, ISSN 0894-1777, doi:10.1016/j.expthermflusci.2012.05.012.

[37] R. Mei, Velocity fidelity of flow tracer particles, Experiments in fluids 22 (1) (1996) 1–13.

[38] M. Amielh, T. Djeridane, F. Anselmet, L. Fulachier, Velocity near-field of variable density turbulent jets, International Journal of Heat and Mass Transfer 39 (10) (1996) 2149 – 2164, ISSN 0017-9310, doi:10.1016/0017-9310(95)00294-4.

[39] G. Xu, R. Antonia, Effect of different initial conditions on a turbulent round free jet, Experiments in Fluids 33 (5) (2002) 677–683, ISSN 1432-1114, doi:10.1007/s00348-002-0523-7.